Stalactite growth as a free-boundary problem

Martin B. Short
Department of Physics, University of Arizona, Tucson, Arizona 85721

James C. Baygents
Department of Chemical and Environmental Engineering and Program in Applied Mathematics,
University of Arizona, Tucson, Arizona 85721

Raymond E. Goldstein[a]
Department of Physics, Program in Applied Mathematics, and B105 Institute, University of Arizona,
Tucson, Arizona 85721

Stalactites, the most familiar structures found hanging from the ceilings of limestone caves, grow by the precipitation of calcium carbonate from within a thin film of fluid flowing down their surfaces. We have recently shown [M. B. Short, J. C. Baygents, J. W. Beck, D. A. Stone, R. S. Toomey III, and R. E. Goldstein, "Stalactite growth as a free-boundary problem: A geometric law and its Platonic ideal," Phys. Rev. Lett. **94**, 018501 (2005)] that the combination of thin-film fluid dynamics, calcium carbonate chemistry, and carbon dioxide diffusion and outgassing leads to a local geometric growth law for the surface evolution which quantitatively explains the shapes of natural stalactites. Here we provide details of this free-boundary calculation, exploiting a strong separation of time scales among that for diffusion within the layer, contact of a fluid parcel with the growing surface, and growth. When the flow rate, the scale of the stalactite, and the chemistry are in the ranges typically found in nature, the local growth rate is proportional to the local thickness of the fluid layer, itself determined by Stokes flow over the surface. Numerical studies of this law establish that a broad class of initial conditions is attracted to an ideal universal shape, whose mathematical form is found analytically. Statistical analysis of stalactite shapes from Kartchner Caverns (Benson, AZ) shows excellent agreement between the average shape of natural stalactites and the ideal shape. Generalizations of these results to nonaxisymmetric speleothems are discussed. © *2005 American Institute of Physics*. [DOI: 10.1063/1.2006027]

I. INTRODUCTION

References to the fascinating structures found in limestone caves, particularly stalactites, are found as far back in recorded history as the writings of the Elder Pliny in the first century A.D.[1] Although the subject of continuing inquiry since that time, the chemical mechanisms responsible for growth have only been well-established since the 19th century. These fundamentally involve reactions within the thin fluid layer that flows down speleothems, the term which refers to the whole class of cave formations. As water percolates down through the soil and rock above the cave, it becomes enriched in dissolved carbon dioxide and calcium, such that its emergence into the cave environment, where the partial pressure of CO_2 is lower, is accompanied by outgassing of CO_2. This, in turn, raises the pH slightly, rendering calcium carbonate slightly supersaturated. Precipitation of $CaCO_3$ adds to the growing speleothem surface. These chemical processes are now understood very well, particularly so from the important works of Dreybrodt,[2] Kaufmann,[3] and Buhmann and Dreybrodt[4] which have successfully explained the characteristic growth rates seen in nature, typically fractions of a millimeter per year.

Surprisingly, a comprehensive translation of these processes into mathematical laws for the growth of speleothems has been lacking. By analogy with the much studied problems of crystal growth in solidification, interface motion in viscous fingering, and related phenomena,[5] it would seem only natural for the dynamics of speleothem growth to have been considered as a free-boundary problem. Yet, there have only been a few attempts at this, for the case of stalagmites,[2–4,6] and they have not been completely faithful to the interplay between fluid mechanics and geometry which must govern the growth. This has left unanswered some of the most basic questions about stalactites (Fig. 1), such as why they are so long and slender, like icicles. Also like icicles,[7–9] speleothem surfaces are often found to have regular ripples of centimeter-scale wavelengths, known among speleologists as "crenulations."[10] No quantitative theory for their appearance has been proposed.

Recently, we presented the first free-boundary approach to the axisymmetric growth of stalactites.[11] In this, we derived a law of motion in which the local growth rate depends on the radius and inclination of the stalactite's surface. This law holds under a set of limiting assumptions valid for typical stalactite growth conditions. Numerical studies of this surface dynamics showed the existence of an attractor in the space of shapes, toward which stalactites will be drawn regardless of initial conditions. An analysis of the steadily

[a] Author to whom correspondence should be addressed; electronic mail: gold@physics.arizona.edu

FIG. 1. Stalactites in Kartchner Caverns. Scale is 20 cm.

TABLE I. Stalactite growth conditions and properties.

Parameter	Symbol	Value
Length	ℓ	10–100 cm
Radius	R	5–10 cm
Fluid film thickness	h	10 μm
Fluid velocity	u_c	1–10 mm/s
Reynolds number	Re	0.01–1.0
Growth rate	v	1 cm/century
Diffusion time	τ_d	0.1 s
Traversal time	τ_t	100 s
Growth time	τ_g	10^6 s
Forward reaction constant	k_+	0.1 s^{-1}
Backward reaction constant	k'_-	10^{-3} s^{-1}
Henry's law constant	H	0.01

properties of an attractor whose details are described in Sec. VII. The procedure by which a detailed comparison was made with stalactite shapes found in Kartchner Caverns is presented in Sec. VIII. Finally, Sec. IX surveys important generalizations which lie in the future, including azimuthally modulated stalactites and the more exotic speleothems such as draperies. Connections to other free-boundary problems in precipitative pattern formation are indicated, such as terraced growth at hot springs.

II. SPELEOTHEM GROWTH CONDITIONS

Here we address gross features of the precipitation process, making use of physical and chemical information readily obtained from the standard literature, and also, for the case of Kartchner Caverns in Benson, AZ, the highly detailed study[12] done prior to the development of the cave for public access. This case study reveals clearly the *range* of conditions which may be expected to exist in many limestone caves (see Table I). It is a typical rule of thumb that stalactite elongation rates v are on the order of 1 cm/century, equivalent to the remarkable rate of $\sim$2 Å/min. One of the key issues in developing a quantitative theory is the extent of depletion of calcium as a parcel of fluid moves down the surface. An estimate of this is obtained by applying the elongation rate v to a typical stalactite, whose radius at the ceiling might be $R \sim 5$ cm. We can imagine the elongation in a time τ to correspond to the addition of a disk at the attachment point, so $\pi R^2 v \tau \sim 80$ cm^3 or $\sim$200 g of CaCO$_3$ (or $\sim$80 g of Ca) is added per century, the density of CaCO$_3$ being 2.7 g/cm^3. Now, the volumetric flow rate of water over stalactites can vary enormously,[12] but in wet caves it is typically in the range of 10–10^3 cm^3/h. If we adopt a conservative value of $\sim$50 cm^3/h, the volume of water that flows over the stalactite in a century is $\sim$44 000 l. A typical concentration of calcium dissolved in solution is 150 ppm (mg/l), so the total mass of calcium in that fluid volume is 6.6 kg, yielding a fractional precipitation of $\sim$0.01. Clearly, depletion of calcium through precipitation does not significantly alter the chemistry from the top to the bottom of stalactites. Indeed, since stalagmites so often form below stalactites, there must be plenty of calcium carbonate still
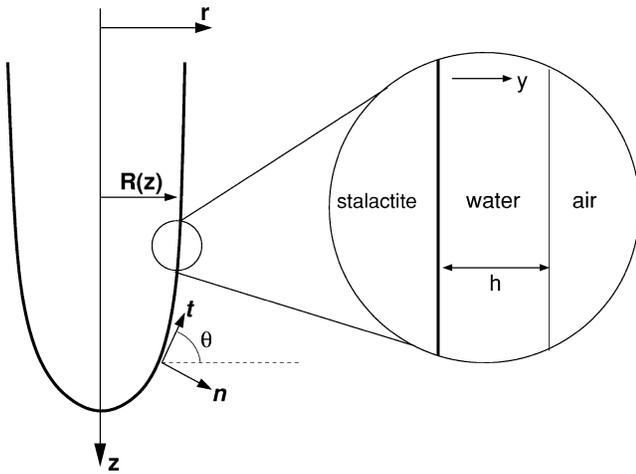
growing shape revealed it to be described by a universal, parameter-free differential equation, the connection to an actual stalactite being through an arbitrary magnification factor. As with the Platonic solids of antiquity—the circle, the square, etc.—which are ideal forms independent of scale, this too is a Platonic ideal. Of course, the shape of any single real stalactite will vary from this ideal in a variety of ways due to instabilities such as those producing crenulations, inhomogeneous cave conditions, unidirectional airflow, etc. Mindful of this, we found that an average of natural stalactites appropriately washes out these imperfections, and compares extremely well with the Platonic ideal. Our purpose in this paper is to expand on that brief description by offering much greater detail in all aspects of the analysis.

Section II summarizes the prevailing conditions of speleothem growth, including fluid flow rates, concentrations of carbon dioxide and dissolved calcium which determine the important time scales, and the relevant Reynolds number. In Sec. III we exploit the strong separation of three times scales to derive the asymptotic simplifications important in subsequent analysis. A detailed study of the linked chemical and diffusional dynamics is presented in Sec. IV, culminating in the local growth law and a measure of the leading corrections. That local law is studied analytically in Sec. V and numerically in Sec. VI, where we establish the existence and

FIG. 2. Geometry of the surface of a stalactite. The tangent and normal vectors, along with the tangent angle θ, are defined.
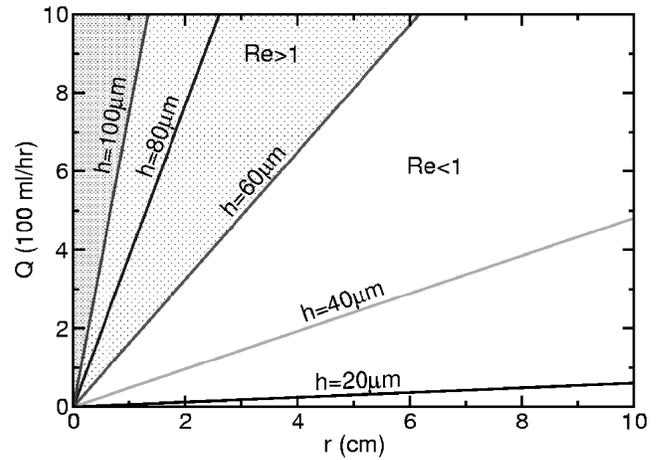

FIG. 3. Contour plot of fluid layer thickness h for various stalactite radii and fluid flow rates evaluated at $\theta = \pi/2$. At a thickness of 60 μm, the Reynolds number approaches unity, and increases with increasing thickness. The shaded area beginning at a thickness of 100 μm denotes the region in which diffusion time across the fluid layer is comparable to the time of the slowest relevant reaction.

available in the drip water for precipitation to occur.

Next, we establish the properties of the aqueous fluid layer on the stalactite surface by considering a cylindrical stalactite of radius R, length ℓ, and coated by a film of thickness h. Visual inspection of a growing stalactite confirms that $h \ll R$ over nearly the entire stalactite, except near the very tip where a pendant drop periodically detaches. Given the separation of length scales, we may deduce the velocity profile in the layer by assuming a flat surface. Let y be a coordinate perpendicular to the surface and θ the tangent angle with respect to the horizontal (Fig. 2). The Stokes equation for gravity-driven flow, $\nu d^2 u/dy^2 = g \sin \theta$, with $\nu = 0.01$ cm^2/s the kinematic viscosity of water, coupled with no-slip and stress-free boundary conditions, respectively, at the solid-liquid and liquid-air interfaces, is solved by the profile

$$u(y) = u_c \left[2\frac{y}{h} - \left(\frac{y}{h}\right)^2 \right], \tag{1}$$

where

$$u_c \equiv \frac{gh^2 \sin \theta}{2\nu} \tag{2}$$

is the maximum velocity, occurring at the free surface. It is important to note that the extremely high humidity typically in the cave assures that evaporation does not play a significant role and so the fluid flux across any cross section is independent of the position along the stalactite. That volumetric fluid flux,

$$Q = 2\pi R \int_0^h u(y) dy = \frac{2\pi gRh^3 \sin \theta}{3\nu}, \tag{3}$$

allows us to solve for h and u_c in terms of the observables Q and R. Measuring Q in cm^3/h and R in centimeters, we find

$$h = \left(\frac{3Q\nu}{2\pi gR \sin \theta}\right)^{1/3} \simeq 11 \ \mu\text{m} \left(\frac{Q}{R \sin \theta}\right)^{1/3}, \tag{4}$$

$$u_c = \frac{gh^2 \sin \theta}{2\nu} \simeq 0.060 \text{ cm s}^{-1} \left(\frac{Q^2 \sin \theta}{R^2}\right)^{1/3}. \tag{5}$$

With the typical flow rates mentioned above and R in the range of 1–10 cm, h is tens of microns and the surface velocities below several mm/s. The Reynolds number on the scale of the layer thickness h is

$$\text{Re} = \frac{u_c h}{\nu} \sim 0.007 \frac{Q}{R}. \tag{6}$$

Using again the typical conditions and geometry, this is much less than unity, and the flow is clearly laminar. Figure 3 is a guide to the layer thickness as a function of Q and R, and the regime in which the Reynolds number approaches unity—only for very thin stalactites at the highest flow rates. The rule for the fluid layer thickness (4) does not hold very near the stalactite tip, where, as mentioned earlier, pendant drops form and detach. Their size is set by the capillary length $l_c = (\sigma/\rho g)^{1/2} \sim 0.3$ cm, where $\sigma \approx 80$ ergs/cm^2 is the air-water surface tension.

III. SEPARATION OF TIME SCALES

Based on the speleothem growth conditions, we can now see that there are three very disparate time scales of interest. The shortest is the scale for diffusional equilibration across the fluid layer,

$$\tau_d = \frac{h^2}{D} \sim 0.1 \text{ s}, \tag{7}$$

where $D \sim 10^{-5}$ cm^2/s is a diffusion constant typical of small aqueous solutes. Next is the traversal time, the time for a parcel of fluid to move the typical length of a stalactite,

$$\tau_t = \frac{\ell}{u_c} \sim 10^2 \text{ s}. \tag{8}$$

Third is the time scale for growth of one fluid layer depth,

$$\tau_g = \frac{h}{v} \sim 10^6 \text{ s.} \tag{9}$$

Inasmuch as the off gassing of CO_2 leads to the precipitation of $CaCO_3$, the concentration distributions of these two chemical species are of interest in the aqueous film. Because the traversal time scale is much less than that for growth, we shall see that solute concentration variations tangent to the growing surface will be negligible and this ultimately permits us to derive a local geometric growth law that governs the evolution of the speleothem shape. To illustrate our approximations, we begin by considering the distribution of Ca^{2+} in a stagnant fluid layer of thickness h. If C and D, respectively, denote the concentration and diffusivity of that species, then

$$\frac{\partial C}{\partial t} = D \frac{\partial^2 C}{\partial y^2}. \tag{10}$$

We require

$$\left.\frac{\partial C}{\partial y}\right|_h = 0 \text{ and } D \left.\frac{\partial C}{\partial y}\right|_0 = F, \tag{11}$$

where the deposition rate F at the solid-liquid boundary ($y=0$) is presumed to depend on the local supersaturation $C - C_{\text{sat}}$. For the sake of discussion, we set

$$F = \gamma(C - C_{\text{sat}}), \tag{12}$$

where γ is a rate constant with units of length/time. Equation (12) implicitly introduces a deposition time scale

$$\tau_{\text{dep}} = \frac{h}{\gamma} \tag{13}$$

that is related to τ_g. Because the observed growth rate of stalactites is so low, for the time being we take $\tau_{\text{dep}} \gg \tau_t \gg \tau_d$. Toward the end of Sec. IV we obtain an expression for F that confirms this ordering of time scales and makes it apparent that γ depends on the acid-base chemistry of the liquid film.

If we define a dimensionless concentration

$$\Theta \equiv \frac{C - C_{\text{sat}}}{C_0 - C_{\text{sat}}}, \tag{14}$$

where C_0 is the initial concentration of the solute in the liquid, we can write Eq. (10) as

$$\frac{\partial^2 \Theta}{\partial y^2} = N \frac{\partial \Theta}{\partial t}, \tag{15}$$

where time t is now scaled on τ_{dep} and the coordinate y is scaled on h. The parameter

$$N \equiv \frac{\gamma h}{D} \tag{16}$$

is a dimensionless group that weighs the relative rates of deposition and diffusion. The boundary conditions become

$$\left.\frac{\partial \Theta}{\partial y}\right|_1 = 0 \text{ and } \left.\frac{\partial \Theta}{\partial y}\right|_0 = N\Theta. \tag{17}$$

Though it is possible to write out an analytical solution to Eqs. (15)–(17), we elect to construct an approximate solution by writing

$$\Theta(y,t) = \bar{\Theta}(t) + N\Theta'(y,t), \tag{18}$$

which is useful when $N \ll 1$, as it is here. $\bar{\Theta}(t)$ represents, to leading order in N, the mean concentration of solute in the fluid layer. Upon substituting (18) into (15)–(17), one obtains

$$\bar{\Theta}(t) = A e^{-t}, \tag{19}$$

where A is an O(1) constant. At short times then, $\bar{\Theta}(t) \simeq A(1-t)$ and $\partial \Theta / \partial t \sim -A$. This means the time rate of change of the solute concentration is constant, and there is little depletion of the solute, on time scales that are long compared to τ_d but short compared to τ_{dep}. This latter point concerning solute depletion and time scales will become more important as we consider the role of advection in the film.

Consider again diffusion of the solute across a liquid film of thickness h, but now suppose that the liquid flows along the solid surface, which is taken to be locally flat and characterized by a length scale $\ell \gg h$ in the direction of the flow. If the flow of the liquid is laminar, the (steady) balance law for the solute (Ca^{2+}) reads as

$$u(y)\frac{\partial C}{\partial x} = D\frac{\partial^2 C}{\partial y^2}. \tag{20}$$

Here diffusion in the x direction has been neglected. In dimensionless form, Eq. (20) is

$$Nf(y)\frac{\partial \Theta}{\partial x} = \frac{\partial^2 \Theta}{\partial y^2}, \tag{21}$$

where x has been scaled on $u_c h / \gamma$ and $f(y) = 2y - y^2$. Note that the small parameter N appears on the left-hand side of (20), implying that advection plays a lesser role than one might anticipate from a cursory evaluation of the Peclet number,

$$\text{Pe} = \frac{u_c h}{D} \sim 7\frac{Q}{R}, \tag{22}$$

which is $\sim 10 - 100$. This is, of course, due to the fact that the gradient in concentration is nearly perpendicular to the fluid velocity field, i.e., the extremely low deposition rate does not lead to a significant reduction in calcium concentration along the length of the stalactite. Boundary conditions (17) still apply and the problem statement is made complete by the requirement that Θ be unity at $x=0$.

To construct an approximate solution to Eq. (21), we write

$$\Theta \equiv \Theta_b(x) + N\Theta'(x,y), \tag{23}$$

where

$$\Theta_b(x) \equiv \frac{\int_0^1 f(y)\Theta(x,y)dy}{\int_0^1 f(y)dy} \tag{24}$$

is the bulk average concentration of the solute at position x. Substituting (23) into (21) yields

$$\Theta_b(x) = A_b e^{-3/2x}, \tag{25}$$
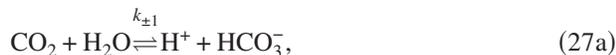
where A_b is unity if $\Theta(0,y)=1$.

Recall that the x coordinate is scaled on $u_c h/\gamma$. This means $x \ll 1$ as long as $\ell \ll u_c h/\gamma$ or, equivalently, $\tau_t \ll \tau_{dep}$. The bulk concentration Θ_b is thus

$$\Theta_b(x) \simeq A_b\left(1 - \frac{3}{2}x\right), \tag{26}$$

indicating that, to leading order, the concentration of the solute in the film diminishes linearly with position, i.e., $\partial\Theta/\partial x$ is approximately constant, which is analogous to the behavior obtained for the stagnant film. More importantly, Eq. (26) reveals the approximate functional form for the calcium depletion and verifies the existence of a length scale over which significant depletion occurs that is much greater than typical stalactite lengths.

IV. CHEMICAL KINETICS AND THE CONCENTRATION OF CO_2

Deposition of $CaCO_3$ is coupled to the liquid-phase concentration of CO_2 through the acid-base chemistry of the film. As the pH of the liquid rises, the solubility of $CaCO_3$ decreases. Much work has been done to determine the rate limiting step in the chemistry of stalactite growth under various conditions.[2–4] For typical concentrations of chemical species, an important conclusion is that the slowest chemical reactions involved in the growth are those that couple carbon dioxide to bicarbonate,

$$CO_2 + H_2O \overset{k_{\pm 1}}{\rightleftharpoons} H^+ + HCO_3^-, \tag{27a}$$

$$CO_2 + OH^- \overset{k_{\pm 2}}{\rightleftharpoons} HCO_3^-. \tag{27b}$$

All other chemical reactions are significantly faster than these and can be considered equilibrated by comparison. It is also critical to note that these reactions are directly coupled to the deposition process; for each molecule of $CaCO_3$ that adds to the surface of the crystal, pathways (27a) and (27b) must generate one molecule of CO_2, which then exits the liquid and diffuses away in the atmosphere. We express the local rate of production of CO_2 by chemical reaction as

$$R_{CO_2} = k_-[HCO_3^-] - k_+[CO_2], \tag{28}$$

where

$$k_- \equiv k_{-1}[H^+] + k_{-2}, \tag{29a}$$
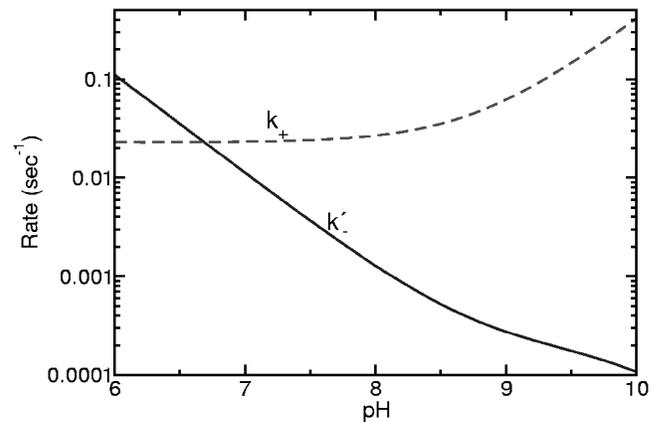

FIG. 4. Values for k_+ and k'_- [Eq. (51)] as functions of pH are shown as dashed and solid lines, respectively. Note that k_+ is much larger than k'_- at pH values typical of caves ($\sim$9), so $[Ca^{2+}]$ must be significantly larger than $[CO_2]$ for growth to occur.

$$k_+ \equiv k_{+1} + k_{+2}[OH^-]. \tag{29b}$$

The pH dependence of the rate constant k_+ (which is much greater than k_-) is shown in Fig. 4. The inverse of this constant defines an additional time scale. At a pH typical of cave water ($\sim$9), the value of k_+ is $\sim$0.1 s^{-1}, giving a chemical reaction time of about 10 s, much greater than the diffusional time scale τ_d. This implies that variations from the average of $[CO_2]$ (or of other chemical species) in the normal direction within the fluid layer will be quite small. The two time scales are not of comparable magnitude until the thickness reaches $\sim$ 100 μm, significantly thicker than typically seen.

The dependence of the precipitation rate on fluid layer thickness is crucial; we follow and extend an important earlier work[4] to derive this. As previously noted, the dynamics of CO_2 plays a critical role in stalactite formation, and the growth of the surface can be found directly from the amount of carbon dioxide leaving the fluid layer into the atmosphere. To that end, we begin with the full reaction-diffusion equation for $[CO_2]$ within the fluid layer, taken on a plane with coordinates x and y tangent and normal to the surface, respectively. That is,

$$\frac{\partial C}{\partial t} + u\frac{\partial C}{\partial x} + w\frac{\partial C}{\partial y} = D\left(\frac{\partial^2 C}{\partial y^2} + \frac{\partial^2 C}{\partial x^2}\right) - k_+C + k_-[HCO_3^-], \tag{30}$$

where $C=[CO_2]$, u and w are the fluid velocity components in the x and y directions, and $D \sim 10^{-5}$ cm^2/s is the diffusion constant associated with CO_2 in water. We now stipulate that only an equilibrium solution is desired, so the partial time derivative will be ignored. We also note that, insofar as the plane is considered flat, the velocity w will be zero everywhere, eliminating a second term. Finally, we rescale quantities as

$$x = \ell\tilde{x}, \quad y = h\tilde{y}, \quad u = u_c\tilde{u}, \quad C = C_0(1 + \phi). \tag{31}$$

Then, omitting the tildes, Eq. (30) can be rewritten as

$$\frac{\tau_d}{\tau_t}u\frac{\partial\phi}{\partial x} = \frac{\partial^2\phi}{\partial y^2} + \left(\frac{h}{\ell}\right)^2\frac{\partial^2\phi}{\partial x^2} + \delta^2(\omega - \phi), \tag{32a}$$

$$\delta \equiv \sqrt{\frac{h^2 k_+}{D}}, \tag{32b}$$

$$\omega \equiv \frac{k_-[HCO_3^-]}{k_+[CO_2]_0} - 1. \tag{32c}$$

Now, since both h/ℓ and τ_d/τ_t are $\sim 10^{-4}$, we will ignore the terms corresponding to diffusion and advection in the x direction. This is further justified by the estimation above regarding the very low fractional depletion of Ca^{2+} as the fluid traverses the stalactite; there is clearly very little change in the concentrations of species from top to tip. The parameter $\delta \sim 10^{-1}$, so we will desire a solution to lowest order in δ only. Furthermore, as δ represents the influence of chemical reactions in comparison to diffusion, it is clear that for very small δ, the concentrations of species will vary only slightly (order of δ^2 at most) from their average throughout the layer. Indeed, the definition of δ indicates that there is an important characteristic distance in this problem, the reaction length

$$\ell_r = \sqrt{\frac{D}{k_+}} \sim 100 \ \mu m. \tag{33}$$

When the layer thickness is smaller than ℓ_r the concentration profile is nearly constant; beyond ℓ_r it varies significantly. This criterion is illustrated in Fig. 3. To lowest order in δ, we need not account for the fact that $[HCO_3^-]$ and $[H^+]$ are functions of y, and instead simply use their average values. The result of these many approximations is the equation

$$\frac{\partial^2 \phi}{\partial y^2} = \delta^2 (\phi - \omega). \tag{34}$$

The first boundary condition imposed on Eq. (34) is that of zero flux of CO_2 at the stalactite surface. Second, we demand continuity of flux between the fluid and atmosphere at the surface separating the two. Third, the concentration of CO_2 in the water at the free fluid surface is proportional to the atmospheric concentration at the same position, the proportionality constant being that of Henry's law.[16] Finally, the atmospheric concentration approaches a limiting value $[CO_2]_\infty$ far from the stalactite. Since the solution to Eq. (34) is dependent upon the atmospheric carbon dioxide field $[CO_2]_a$, we stipulate that this quantity obeys Laplace's equation

$$\nabla^2 [CO_2]_a = 0, \tag{35}$$

as is true for a quiescent atmosphere.

At this point, we alter the geometry of the model to that of a sphere covered with fluid (Fig. 5), as Laplace's equation is more amenable to an exact solution in these coordinates. We do not anticipate that this will affect the model in any significant way, as we have already condensed the problem to variations of the CO_2 concentrations in the direction normal to the stalactite surface only. This approximation would be problematic if atmospheric diffusion played a significant role; this turns out to be not the case, as explained below. In these new coordinates, the atmospheric carbon dioxide concentration is
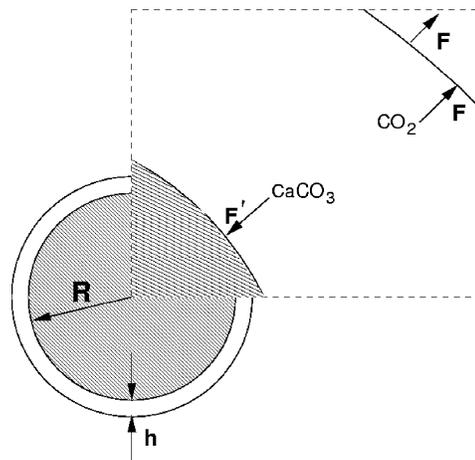

FIG. 5. Spherical model for calculating the growth rate. F and F' are the magnitudes of the fluxes of carbon dioxide and calcium carbonate.

$$[CO_2]_a = [CO_2]_\infty + \frac{A}{r}, \tag{36}$$

where r is the radial position relative to the center of the sphere and A is a constant to be determined. To first order in $\epsilon \equiv h/R \sim 10^{-3}$ the value of $[CO_2]_a$ at the water-air interface, $r = R + h$, is

$$[CO_2]_a|_{R+h} = [CO_2]_\infty + (1 - \epsilon)\frac{A}{R}. \tag{37}$$

Likewise, the flux of CO_2 exiting the fluid at this interface is found to be

$$F = (1 - 2\epsilon)\frac{D_a A}{R^2}, \tag{38}$$

where $D_a \sim 10^{-2} \ cm^2/s$ is the atmospheric diffusion coefficient of carbon dioxide.

Now we turn to the aqueous $[CO_2]$. If we express (34) in spherical coordinates with the rescaling $r = R + hy$, and expand to first order in ϵ we obtain

$$\frac{\partial^2 \phi}{\partial y^2} + 2\epsilon \frac{\partial \phi}{\partial y} = \delta^2 (\phi - \omega). \tag{39}$$

The first boundary condition of zero flux at the stalactite surface can be expressed as

$$\left. \frac{\partial \phi}{\partial y} \right|_{y=0} = 0. \tag{40}$$

The Henry law boundary condition is rewritten as

$$\phi(1) = (1 - \epsilon)\frac{A}{R[CO_2]_\infty}, \tag{41}$$

where we have taken $[CO_2]_0$ to be $H[CO_2]_\infty$. Finally, using (38) and our definition of $[CO_2]_0$, the condition of flux continuity between the fluid and atmosphere can be written as

$$\left. \frac{\partial \phi}{\partial y} \right|_{y=1} = -\epsilon \frac{D_a A}{DRH[CO_2]_\infty}. \tag{42}$$

Eliminating A between Eqs. (41) and (42) we obtain

$$\left.\frac{\partial \phi}{\partial y}\right|_{y=1} = -\epsilon \frac{D_a}{DH} \phi(1). \tag{43}$$

After straightforwardly solving Eq. (39) subject to the boundary conditions (40) and (43), we expand to lowest order in δ and first order in ϵ. From this, we find that the function ϕ is

$$\phi = \omega \delta^2 \left(\frac{1-y^2}{2} - \epsilon \frac{1-y^3}{3} + \frac{DH}{D_a} \frac{1-\epsilon-\epsilon^2}{\epsilon} \right). \tag{44}$$

We then easily calculate the amount of carbon dioxide leaving the fluid by multiplying the CO_2 flux by the surface area of the outside of the liquid layer. The final step is to equate the amount of CO_2 leaving with the amount of $CaCO_3$ adding to the surface and divide by the surface area of the sphere to find the $CaCO_3$ flux. The result is

$$F' = h(k_-[HCO_3^-] - k_+ H[CO_2]_\infty)(1 + \epsilon). \tag{45}$$

We see then that atmospheric diffusion is negligible at lowest order and that the flux is directly proportional to the fluid layer thickness. Finally, though the spherical approximation used above is useful, it is not strictly necessary, and the calculations can be repeated using a cylindrical model instead. The result in this geometry is

$$F' = h(k_-[HCO_3^-] - k_+ H[CO_2]_\infty)(1 - \epsilon/2), \tag{46}$$

differing from the spherical model only at order ϵ. As we will neglect this term for the remainder of the paper, the choice of geometry is irrelevant.

As information regarding typical $[HCO_3^-]$ is less available than that regarding $[Ca^{2+}]$, we wish to reexpress Eq. (45) in terms of the calcium ion concentration. This is readily accomplished by first imposing an electroneutrality condition on the fluid at any point,

$$2[Ca^{2+}] + [H^+] = 2[CO_3^{2-}] + [HCO_3^-] + [OH^-]. \tag{47}$$

Next, we note that $[OH^-]$ and $[H^+]$ are related through the equilibrium constant of water K_W, and that $[CO_3^{2-}], [H^+]$, and $[HCO_3^-]$ are related through another equilibrium constant, K. Hence, we can express $[HCO_3^-]$ solely in terms of these constants, $[Ca^{2+}]$, and $[H^+]$ as

$$[HCO_3^-] = \frac{2[Ca^{2+}] + (1-\beta)[H^+]}{1 + 2\alpha}, \tag{48}$$

where

$$\beta = \frac{K_W}{[H^+]^2}, \quad \alpha = \frac{K}{[H^+]}. \tag{49}$$

Upon substitution of this formula into Eq. (45), we obtain (ignoring the order ϵ correction)

$$F' = h(k'_-[Ca^{2+}] + k_0[H^+] - k_+ H[CO_2]_\infty), \tag{50}$$

$$k'_- = \frac{2}{1+2\alpha}k_-, \quad k_0 = \frac{1-\beta}{1+2\alpha}k_-. \tag{51}$$

As one can now see *a posteriori*, the calcium ion flux is indeed given by a formula of the form supposed in Eq. (12), where the values of γ and C_{sat} are given by
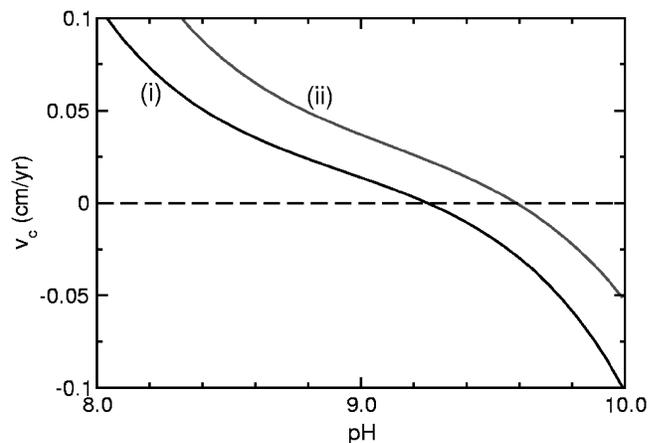

FIG. 6. Growth velocity v_c vs pH, using CO_2 partial pressure in the cave of 3×10^{-4} atm, a temperature of 20 °C, and (i) $\overline{[Ca^{2+}]}$ of 200 ppm and volumetric fluid flow $Q = 30$ cm^3/h and (ii) $\overline{[Ca^{2+}]} = 500$ ppm and $Q = 5$ cm^3/h. The formulas for the constants are taken from Ref. 4.

$$\gamma = hk'_-, \quad C_{sat} = \frac{k_+}{k'_-} H[CO_2]_\infty - \frac{k_0}{k'_-}[H^+]. \tag{52}$$

With these definitions, $\tau_{dep} = 1/k'_- \sim 10^4$, and our previous time-scale orderings are vindicated. In addition, the expression for C_{sat} is consistent with the underlying chemical kinetics.

V. LOCAL GEOMETRIC GROWTH LAW

The two ingredients of the local growth law are now at hand: the relation (50) for the flux as a function of fluid layer thickness and internal chemistry, and the result (4) connecting the layer thickness to the geometry and imposed fluid flux Q. Combining the two, we obtain at leading order a *geometrical* law for growth. It is most appropriately written as a statement of the growth velocity **v** along the unit normal to the surface ($\hat{\mathbf{n}}$ in Fig. 2),

$$\hat{\mathbf{n}} \cdot \mathbf{v} = v_c \left(\frac{\ell_Q}{r \sin \theta} \right)^{1/3}. \tag{53}$$

Here, $r(z)$ is the local radius and $\theta(z)$ is the local tangent angle of the surface, and

$$v_c = v_m \ell_Q (k'_-[Ca^{2+}] + k_0[H^+] - k_+ H[CO_2]_\infty) \tag{54}$$

is the characteristic velocity, with v_m being the molar volume of $CaCO_3$, and

$$\ell_Q = \left(\frac{3\nu Q}{2\pi g} \right)^{1/4} \sim 0.01 \text{ cm} \tag{55}$$

a characteristic length. The velocity v_c depends upon the pH not only through $[H^+]$ but also through the definitions of k'_- and k_+, crossing from positive (growth) to negative (dissolution) at a critical pH that depends on the average calcium ion concentration, the partial pressure of CO_2 in the cave atmosphere, and the fluid flux. Figure 6 shows some examples of this behavior. Cave water is often close to the crossing point, implying values for v_c on the order of 0.1 mm/year.
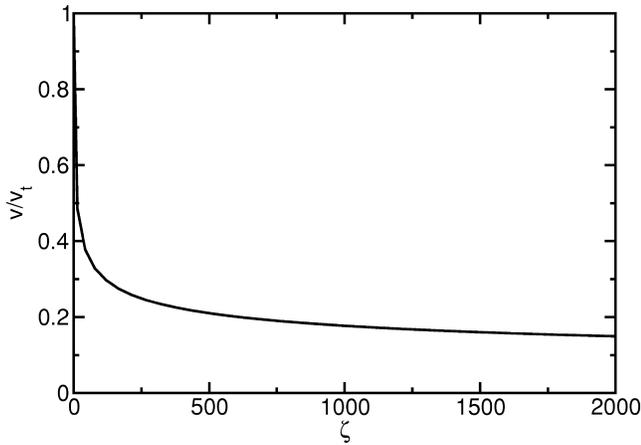
FIG. 7. The dimensionless growth velocity, v/v_t, vs, ζ, defined in Eq. (56), evaluated for the ideal stalactite shape (Fig. 9). Note the precipitous drop away from the stalactite's tip.
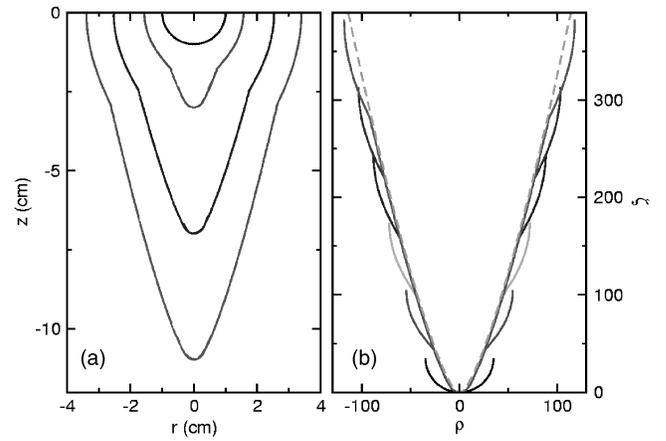

FIG. 8. Numerical results. (a) A rounded initial condition evolves into a fingered shape. (b) Aligning the tips of the growing shapes shows rapid collapse to a common form. Here, the profiles have been scaled appropriately [Eq. (60)] and are shown with the ideal curve (dashed line).

In comparison to many of the classic laws of motion for surfaces, the axisymmetric dynamics (53) is rather unusual. First, unlike examples such as "motion by mean curvature"[13] and the "geometrical" models of interface motion,[14] it depends not on geometric invariants but on the absolute orientation of the surface through the tangent angle, and on the radius r of the surface. As remarked earlier,[11] the fact that it depends on the tangent angle θ is similar to the effects of surface tension anisotropy,[15] but without the periodicity in θ one finds in that case. The variation (Fig. 7) is extreme near the tip, where θ and r are both small, and minor in the more vertical regions, where $\theta \sim \pi/2$ and r is nearly constant.

Note also that the geometric growth law takes the form of a product of two terms, one dependent only upon chemistry, the other purely geometric. This already implies the possibility that while individual stalactites may grow at very different rates as cave conditions change over time (for instance, due to variations in fluid flux, and carbon dioxide and calcium levels), the geometric relationship for accretion does not change. Therein lies the possibility of an underlying common form, as we shall see in subsequent sections.

VI. NUMERICAL STUDIES

In order to understand the shapes produced by the growth law (53), numerical studies were performed to evolve a generic initial condition. The method of these simulations is based on well-known principles.[14] Here, because of the axisymmetric nature of our law, we take the stalactite tangent angle θ to be the evolving variable. The time-stepping algorithm is an adaptive, fourth-order Runge-Kutta method. For simplicity, all simulations were performed with the boundary condition that the stalactite be completely vertical at its highest point (i.e., the cave ceiling). The growth law breaks down very near the tip, where the precipitation dynamics becomes much more complex. However, it is safe to assume that the velocity of the stalactite's tip v_t is a monotonically increasing function of flow rate Q. For the numerics then, velocities at radii smaller than the capillary length are extrapolated from those near this region, with the tip velocity scaling at a rate

greater than $Q^{1/3}$ (this choice will be explained in more detail in Sec. VII). The volumetric fluid flux is a user-defined parameter and sets the value of ℓ_Q.

Figure 8 shows how a shape which is initially rounded develops an instability at its lowest point. The mechanism of the instability follows from the flux conservation that is an integral part of the dynamics. The downward protuberance has a locally smaller radius than the region above and therefore a thicker fluid layer. According to (45) this increases the precipitation rate, enhancing the growing bump. We find numerically that the growing protuberance approaches a uniformly translating shape for a wide range of initial conditions (Fig. 8). The aspect ratio of this shape, defined here as the length ℓ divided by maximum width W, is influenced by the flow rate chosen for the simulation, with a high flow giving a higher aspect ratio stalactite than a low flow for equal stalactite lengths.

VII. THE TRAVELING SHAPE

The asymptotic traveling shape $z(r)$ can be found by noting that the normal velocity (53) at any point on such a surface must equal $v_t \cos \theta$, where, as noted previously, v_t is the tip velocity. Observing that $\tan \theta = dz/dr$, and rescaling symmetrically r and z as

$$\rho \equiv \frac{r}{\ell_Q}\left(\frac{v_t}{v_c}\right)^3 \quad \text{and} \quad \zeta \equiv \frac{z}{\ell_Q}\left(\frac{v_t}{v_c}\right)^3, \tag{56}$$

we find the differential equation

$$\frac{\zeta'(\rho)}{[1 + \zeta'(\rho)^2]^2} - \frac{1}{\rho} = 0. \tag{57}$$

Let us now examine Eq. (57) in detail. A first observation is that for large ζ' the balance of terms is $(\zeta')^{-3} \sim \rho^{-1}$, implying a power law,

$$\zeta \sim \rho^\alpha, \quad \alpha = \tfrac{4}{3}. \tag{58}$$

This particular power can be traced back to the flux relation $Q \sim h^3$, and if this were more generally $Q \sim h^\psi$ then $\alpha = (\psi$
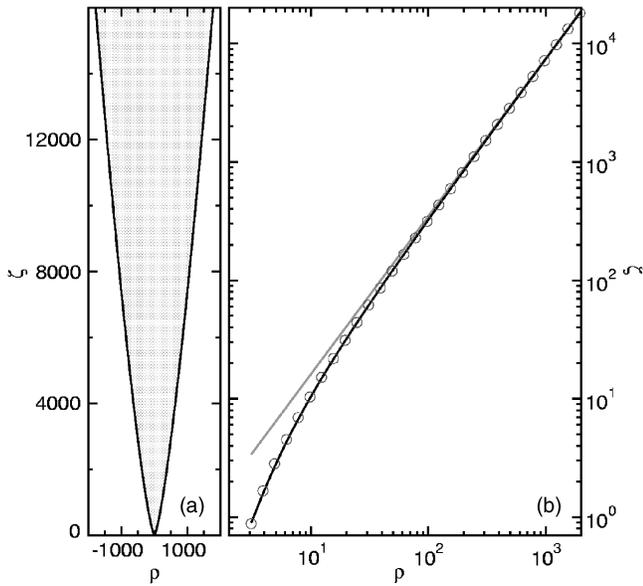
FIG. 9. Platonic ideal of stalactite shapes. (a) The shape is from the numerical integration of Eq. (57). (b) The gray line shows comparison of that integration with the pure power law given by the first term in (59), while the circles represent the complete asymptotic form in (59).

+1)/ψ which is always greater than unity for the physically sensible $\psi > 0$. As this is steeper than linear the associated shape is convex outward, and therefore has an aspect ratio that increases with overall length—just as the classic carrot-like shape of stalactites.

The differential Eq. (57) has some mathematical subtleties. The term involving ζ' vanishes at $\zeta'(\rho)=0$ and also as $\zeta'(\rho)\to\infty$, is positive at all points in between, and has a maximum of magnitude $3\sqrt{3}/16$ at the point $\zeta'(\rho)=1/\sqrt{3}$. The rightmost term will then shift this function downward by an amount $1/\rho$. So, at $\rho=0$, there is no real solution to Eq. (57). Of course, this is acceptable to us because we do not expect the velocity law (53) to be valid exactly at the tip of the stalactite, where capillarity must modify the thickness of the film. As ρ moves away from zero, we first encounter a real solution at $\rho=\rho_m \equiv 16/3\sqrt{3}$, at which point $\zeta'(\rho)$ is equal to $1/\sqrt{3}$. This minimum radius cutoff, which is intrinsic to the mathematics and, therefore, inescapable, should not be confused with the somewhat arbitrary capillary length cutoff used earlier in the numerical studies. For all ρ greater than this minimal ρ_m, there will be two distinct real solutions of the equation for $\zeta'(\rho)$. One solution is a decreasing function of ρ, the other an increasing function. Since the physically relevant shape of a stalactite has a large slope at a large radius, the second root is of greater interest.

The astute reader will notice that Eq. (57) is essentially a fourth-order polynomial equation for $\zeta'(\rho)$, and thus admits an exact solution. This solution is quite complex, though, and does not readily allow for an exact analytic formula for $\zeta(\rho)$, though it is useful for numerical integration. Figure 9 shows the shape so determined. At large values of ρ, this formula can be expanded and integrated to yield the approximation

$$\zeta(\rho) \simeq \tfrac{3}{4}\rho^{4/3} - \rho^{2/3} - \tfrac{1}{3}\ln\rho + \mathcal{O}(\rho^{-2/3}). \qquad (59)$$

It is important to note that this ideal shape is completely parameter-free; all of the details of the flow rate, characteristic velocity, and tip velocity are lost in the rescaling. Hence, the stalactites created by our numerical scheme should all be of the same dimensionless shape, the only difference between them arising from the different magnification factors

$$a \equiv \ell_Q \left(\frac{v_c}{v_t} \right)^3 \qquad (60)$$

that translate that shape into real units. Clearly, when comparing stalactites of equal length, the one with the lower magnification factor will occupy a greater extent of the universal curve, hence it will also have a higher aspect ratio. This explains our earlier choice that the tip velocity should scale at a rate greater than $Q^{1/3}$; with such a scaling, higher flow rates lead to lower magnification factors and higher aspect ratios, as is the case with real stalactites.

VIII. COMPARISONS WITH STALACTITES IN KARTCHNER CAVERNS

In this section we describe a direct comparison between the ideal shape described by the solution to Eq. (57) and real stalactites found in Kartchner Caverns in Benson, AZ. As is readily apparent to any cave visitor, natural stalactites may experience a wide range of morphological distortions; they may be subject to air currents and grow deformed along the direction of flow: they may be part of the sheet-like structures known as "draperies," ripples may form (see below), etc. To make a comparison with theory we chose stalactites not obviously deformed by these processes. Images of suitable stalactites were obtain with a high-resolution digital camera (Nikon D100, 3008×2000 pixels), a variety of telephoto and macrolenses, and flash illumination where necessary. To provide a local scale on each image, a pair of parallel green laser beams 14.5 cm apart was projected on each stalactite.

Let us emphasize again that because the rescalings used to derive Eq. (57) are symmetric in r and z, a direct comparison between actual stalactites and the ideal requires only a global rescaling of the image. Moreover, as the aspect ratio for the ideal increases with the upper limit of integration, our theory predicts that all stalactites will lie on the ideal curve provided the differential equation defining that curve is integrated up to a suitable length. Therefore, we can visually compare stalactite images to the ideal shape rather simply. Figure 10 shows three representative examples of such a direct comparison, and the agreement is very good. Small deviations are noted near the tip, where capillarity effects associated with the pendant drops alter the shape.

For a more precise comparison, we extracted the contours of 20 stalactites by posterizing each image and utilizing a standard edge detection algorithm to obtain $r(z)$ for each [Fig. 11(a)]. The optimal scale factor a for each was found by a least-squares comparison with the ideal function [Fig. 11(b)]. This set of rescaled data was averaged and compared directly to the theoretical curve, yielding the master plot in Fig. 12. The statistical uncertainties grow with distance from
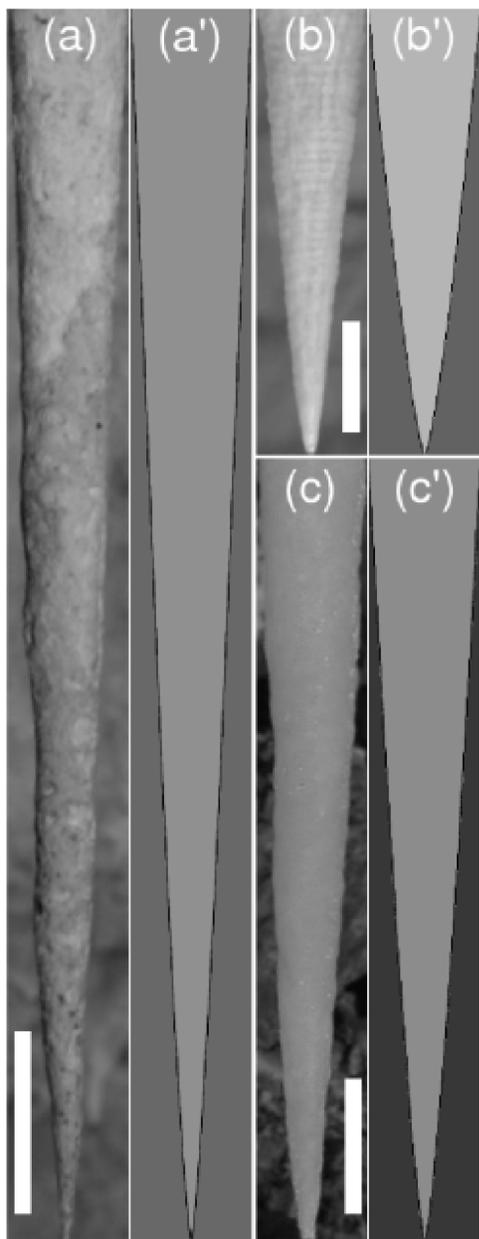
FIG. 10. Comparison between observed stalactite shapes and the Platonic ideal. Three examples [(a)—(c)] are shown, each next to an ideal shape of the appropriate aspect ratio and size [(a′)–(c′)]. Scale bars in each are 10 cm.
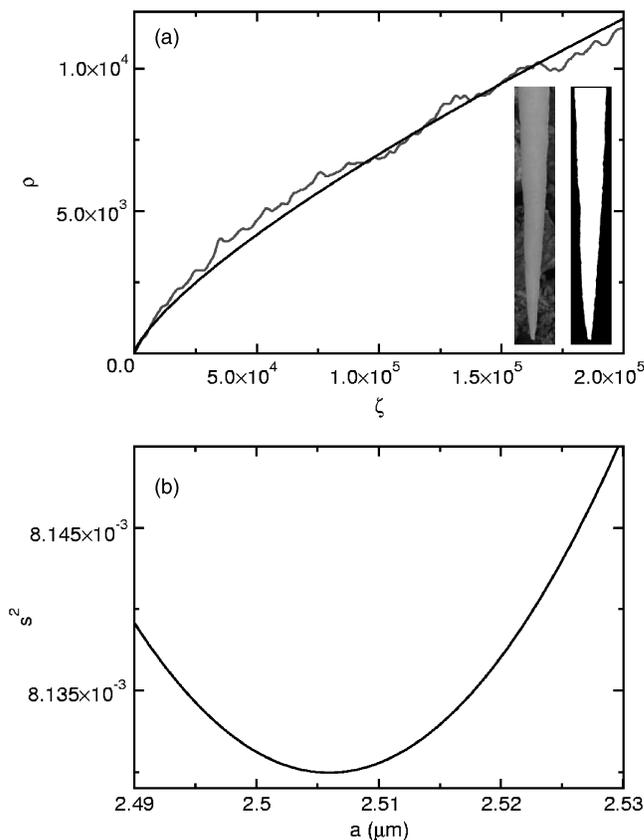

FIG. 11. Analysis of natural stalactites. (a) Posterization of an image to yield a contour, shown with the optimum scaling to match the ideal form. (b) Variance of the fit as a function of the scale factor a, showing a clear minimum.

the stalactite tip because there are fewer long stalactites contributing to the data there. We see that there is excellent agreement between the data and the Platonic ideal, the latter falling uniformly within one standard deviation from the former. A plot of the residuals to the fit, shown in Fig. 13, indicates that there is a small systematic positive deviation near the tip. This is likely traced back to capillary effects ignored in the present calculation. These results show that the essential physics underlying stalactite growth is the spatially varying fluid layer thickness along the surface, which gives rise to extreme enhancement of growth near the tip. The characteristic, slightly convex form is an explicit consequence of the cubic relationship between flux and film thickness.

IX. CONCLUSIONS

The dynamic and geometric results presented here illustrate that the essential physics underlying the familiar shape of stalactites is the locally varying fluid layer thickness controlling the precipitation rate, under the global constraint on that thickness provided by fluid flux conservation. Since so many speleothem morphologies arise from precipitation of calcium carbonate out of thin films of water, it is natural to conjecture that these results provide a basis for a quantitative understanding of a broad range of formations. Generalizations of this analysis to other speleothem morphologies can be divided into two classes: axisymmetric and nonaxisymmetric. Chief among the axisymmetric examples are stalagmites, the long slender structures growing up from cave floors, often directly below stalactites. These present significant complexities not found with stalactites. First, the upper ends of stalagmites are decidedly not pointed like the tips of stalactites, for the fluid drops that impact it do so from such a height as to cause a significant splash, although, when a stalagmite grows close to the stalactite above, it does tend to adopt a mirror-image form, the more so the closer the two are to fusing. Like stalactites, stalagmites and indeed most speleothem surfaces may display centimeter-scale ripples, further emphasizing the importance of a linear stability analysis of the coupled fluid flow and reaction-diffusion dynamics. A key question is why some stalactites display
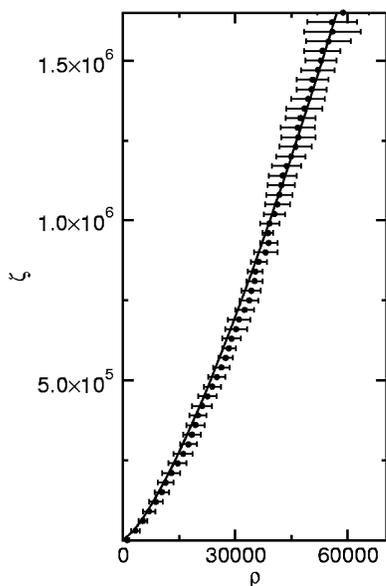
FIG. 12. Master plot of stalactite shapes, rescaled as described in text. The average of 20 stalactites is shown, compared with the ideal (black curve).

FIG. 13. Residuals of the fit to ideal shape, from Fig. 12.

ripples while others do not. This will be discussed elsewhere. Many stalagmites also display a series of wedge-like corrugations on a scale much larger than the crenulations. We conjecture that these may be a signature of a secondary instability, the identification of which would require a fully nonlinear theory to describe the saturated amplitude of crenulations.

Two kinds of nonaxisymmetric forms are of immediate interest, those which arise from instabilities of axisymmetric shapes, and those which are formed by a mechanism with a fundamentally different intrinsic symmetry. A likely physical explanation of these forms is that a small azimuthal perturbation on an inclined surface, effectively a ridge, will accumulate fluid, thereby growing faster. Such deviations from axisymmetry present an interesting challenge for free-boundary theories, for the constraint of global flux conservation translates into a single azimuthal constraint on the variable film thickness at a given height on the speleothem. Formations of fundamentally different symmetry include draperies, sheet-like structures roughly 1 cm thick, with undulations on a scale of 20 cm. These grow typically from slanted ceilings along which flow rivulets of water, and increase in size by precipitation from fluid flowing along the lower edge. That flow is susceptible to the Rayleigh–Taylor instability, and not surprisingly there are often periodic undulations with a wavelength on the order of the capillary length seen on the lower edges of draperies. Since it is known that jets flowing down an inclined plane can undergo a meandering instability, it is likely that the same phenomenon underlies the gentle sinusoidal forms of draperies.

Other structures in nature formed by precipitation from solution likely can be described by a similar synthesis of fluid dynamics and geometric considerations. Examples include the hollow soda straws in caves, whose growth is templated by pendant drops (analogous to tubular growth templated by gas bubbles in an electrochemical setting[16]).
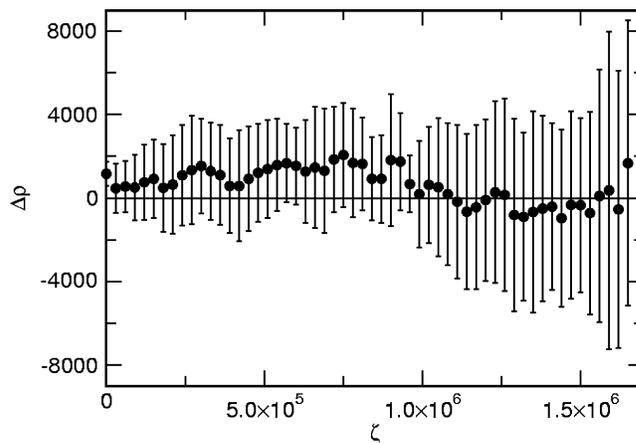
Likewise, the terraces that form at mineral-rich hot springs like those at Yellowstone National Park provide a striking example of precipitative growth from solution. Moreover, the striking similarity between the geometry of stalactites and icicles, and especially the ripples on icicles (as discussed in recent works[7–9]), suggests a commonality in their geometric growth laws. In both cases there is a thin film of fluid flowing down the surface, and a diffusing scalar field (carbon dioxide in the case of stalactites and latent heat for icicles) controlling the growth of the underlying surface. While the extreme separation between diffusional, traversal, and growth time scales found in the stalactite problem likely does not hold in the growth of icicles, that separation appears large enough to allow a significant equivalence between the growth dynamics of icicles and stalactites. Finally we note that it would be desirable to investigate model experimental systems whose time scale for precipitation is vastly shorter than natural stalactites. Many years ago Huff[17] developed one such system based on gypsum. Further studies along these lines would provide a route to real-time studies of a whole range of free-boundary problems in a precipitative pattern formation.

ACKNOWLEDGMENTS

[1]C. Hill and P. Forti, *Cave Minerals of the World* (National Speleological Society, Huntsville, AL, 1997)

[2]W. Dreybrodt, "Chemical kinetics, speleothem growth and climate," Boreas **28**, 347 (1999).

[3]G. Kaufmann, "Stalagmite growth and palaeo-climate: the numerical perspective," Earth Planet. Sci. Lett. **214**, 251 (2003).

[4]D. Buhmann and W. Dreybrodt, "The kinetics of calcite dissolution and precipitation in geologically relevant situations of karst areas. 1. Open system," Chem. Geol. **48**, 189 (1984).

[5]M. C. Cross and P. C. Hohenberg, "Pattern formation outside of equilib-

rium," Rev. Mod. Phys. **65**, 851 (1993).

[6]H. W. Franke, "The theory behind stalagmite shapes," Stud. Speleol. **1**, 89 (1965).

[7]N. Ogawa and Y. Furukawa, "Surface instability of icicles," Phys. Rev. E **66**, 041202 (2002).

[8]K. Ueno, "Pattern formation in crystal growth under parabolic shear flow," Phys. Rev. E **68**, 021603 (2003).

[9]K. Ueno, "Pattern formation in crystal growth under parabolic shear flow. II." Phys. Rev. E **69**, 051604 (2004).

[10]C. A. Hill, "On the waves," Sci. News (Washington, D. C.) **163**, 111 (2003).

[11]M. B. Short, J. C. Baygents, J. W. Beck, D. A. Stone, R. S. Toomey III, and R. E. Goldstein, "Stalactite growth as a free-boundary problem: A geometric law and its platonic ideal," Phys. Rev. Lett. **94**, 018510 (2005).

[12]*Final Report: Environmental and Geologic Studies for Kartchner Caverns State Park*, edited by R. H. Beucher (Arizona Conservation Projects, Tucson, AZ, 1992).

[13]M. Gage and R. S. Hamilton, "The heat equation shrinking convex plane-curves," J. Diff. Geom. **23**, 69 (1986).

[14]R. C. Brower, D. A. Kessler, J. Koplik, and H. Levine, "Geometrical models of interface evolution," Phys. Rev. A **29**, 1335 (1984).

[15]D. A. Kessler, J. Koplik, and H. Levine, "Pattern selection in fingered growth phenomena," Adv. Phys. **37**, 255 (1988).

[16]D. A. Stone and R. E. Goldstein, "Tubular precipitation and redox gradients on a bubbling template," Proc. Natl. Acad. Sci. U.S.A. **101**, 11537 (2004).

[17]L. C. Huff, "Artificial helictites and gypsum flowers," J. Geol. **48**, 641 (1940).